Optimization of K-shell emission in aluminum z-pinch implosions: Theory versus experiment

K. G. Whitney, J. W. Thornhill, J. L. Giuliani, Jr., and J. Davis
Plasma Physics Division, Naval Research Laboratory, Washington, D.C. 20375

L. A. Miles, E. E. Nolting, V. L. Kenyon, W. A. Speicer, J. A. Draper, C. R. Parsons, and P. Dang
Naval Surface Warfare Center, White Oak, Silver Spring, Maryland 20903

R. B. Spielman, T. J. Nash, J. S. McGurn, and L. E. Ruggles
Sandia National Laboratories, Albuquerque, New Mexico 87185

C. Deeney, R. R. Prasad, and L. Warren
Physics International Co., San Leandro, California 94577
(Received 25 March 1994)

Two sets of z-pinch experiments were recently completed at the Saturn and Phoenix facilities of Sandia National Laboratories and the Naval Surface Warfare Center, respectively, using aluminum wire arrays of different wire and array diameters. Measurements of the total x-ray yield from the K shell of aluminum were made. In this paper, a comparison of these measurements is made to both theoretical predictions and to a similar set of earlier measurements that were made at the Double Eagle facility of Physics International Company. These three sets of yield measurements have points of agreement with predicted yields and with each other, but they also show points of mutual disagreement, whose significance is discussed. The data are analyzed using a slightly revised version of a previously published K-shell yield scaling law, and they support the existence of a reasonably well defined region in (load mass)–(implosion velocity) space in which plasma kinetic energy is efficiently converted into K-shell x rays. Furthermore, a correlation is observed between the inferred conversion efficiencies and the times in which the implosions occur relative to the times when each generator's short-circuit current reaches its peak value. Finally, unlike the Double Eagle experiments, the largest measured yields in the new experiments were observed to occur at the upper velocity boundary of the efficient emission region. Moreover, the observed yields are in fairly good quantitative agreement with an earlier scaling law prediction of the maximum K-shell x-ray yield from aluminum as a function of load mass assuming kinetic energy conversion alone.

PACS number(s): 52.25.Nr, 52.55.Ez

I. INTRODUCTION

There are roughly four discernible and possibly overlapping phases to wire-array, z-pinch dynamics. At first, there is an explosion phase, in which the initiation of the pulse-power discharge explodes the wires, setting up an initial plasma state for the second, implosion phase. The implosion is driven by $\mathbf{J}\times\mathbf{B}$ forces as the current discharge continues. When the plasma assembles on axis, a third (thermalization) phase begins. In this phase, the kinetic energy is converted to thermal energy and the plasma rapidly ionizes to ionization stages that are generally inaccessible during implosion. The emission of an intense kilovolt x-ray pulse commences during this third phase of the dynamics. Finally, when the current is sustainable and sufficiently strong to maintain plasma confinement, a fourth heating and compression phase is possible during which x-ray production continues.

Phases 2 and 3 were recently studied theoretically using a series of one dimensional (1D) radiative magnetohydrodynamics (MHD) calculations of aluminum wire-array implosions [1,2] to make detailed x-ray yield predictions. In these calculations, initially uniform and cool shells ($\cong 15$ eV) of plasma that were located, on average, at a radius of 1 cm were accelerated by a prescribed linearly rising current. The current was terminated prior to plasma assembly when the outer radius of the plasma reached 1.4 mm in approximate conformity with experimentally observed z-pinch radii on axis. The calculations followed the plasma dynamics through thermalization during which time a kilovolt x-ray pulse was generated when the aluminum plasma ionized into and radiated from the K shell, i.e., from the hydrogenlike and heliumlike ionization stages.

The basic idea promoted in Ref. [1] was that z-pinch arrays needed to acquire a final kinetic energy per ion K_i in excess of (and usually a small multiple of) a minimum energy $E_{\min}$ in order for the plasma to ionize into and radiate effectively from the K shell. As the atomic number Z of the load is increased, $E_{\min}$ increases roughly as $E_{\min}=1.012Z^{3.662}$ eV/ion. Thus, for aluminum, $E_{\min}$ is approximately 12 keV/ion; whereas for krypton, it is estimated to be 506 keV/ion. Because the plasma radiates effectively from the K shell (and from the L shells of moderate atomic number elements) per ion in units of $E_{\min}$, it is convenient to define a dimensionless parameter

η by $\eta \equiv K_i / E_{\min}$. It should satisfy the criterion $\eta > 1$, i.e., $K_i > 12$ keV/ion for aluminum, since only ion energy in excess of $E_{\min}$ can be radiated from the K shell in a thermal plasma.

The MHD calculations, which are described in Refs. [1] and [2], predicted how the K-shell yields from aluminum varied with m, the imploded array mass per unit length, when η was held constant or with η when m was held constant. For fixed η, it was found that the yield makes a sharp transition from m^2 dependence for small mass loads to an m dependence at large masses. The calculations used classical plasma conductivities, and they produced hard implosions, i.e., implosions in which the plasma assembled on axis at one point in time into a tight pinch of radius on the order of 0.1 mm. In these calculations, a negligible amount of back pressure was developed during the load's acceleration, and a slug model description of the implosion dynamics was found to be accurate.

A set of experiments was subsequently carried out at Physics International Co. [3] (PI) in order to test both the validity of the η criterion and the validity of the yield predictions. They were not designed to hold either m or η constant. Instead, as m was varied, the initial radius of the imploded array, r_0, was changed in order to keep the value of mr_0^2 approximately the same. This condition corresponds roughly to holding the implosion times in the experiments constant. It should also correspond to holding either K_T, the total kinetic energy of the implosion, or the product $m\eta$ roughly constant if the implosions all have the same aspect ratio, i.e, the same ratio of initial array radius to final pinch radius. Consequently, the x-ray scaling relations, derived from the MHD calculations in Ref. [1], predicted that the yields in the PI experiments should have been approximately constant as well. This prediction assumed a fixed fractional conversion ($\sim 35\%$) of kinetic energy into K-shell x rays for all array implosions of different m and r_0 for which $mr_0^2 = \text{const}$.

The PI experiments confirmed that aluminum pinches behave as efficient (approximately bulk) K-shell radiators when the condition $\eta \geq 1$ is satisfied. Moreover, the kinetic energy conversion efficiencies predicted by the calculations were exceeded. However, two important differences between theory and experiment were observed. First, the K-shell yields were not flat, but had a peak for small $\eta \sim 1$, corresponding to a kinetic energy conversion efficiency $> 100\%$—a theoretical impossibility if the only energy input to the plasma is kinetic. Second, the experimental implosions were much softer than the implosions that had been calculated, i.e., they assembled on axis with radii on the order of 1 mm. The first difference suggests that an anomalously high amount of Ohmic heating may have occurred when the current continued to flow on axis. The second points to a conjecture that the experimental plasmas had anomalously high (perhaps MHD turbulence induced) time averaged viscosities and possibly large heat conductivities.

If turbulence is present in experimental implosions (either from $\mathbf{J} \times \mathbf{B}$ shears introduced into the flow by the finite number of return current posts used in the experiments, or from current-driven vorticity generation [4,5], or Rayleigh-Taylor instabilities [6,7]), then its main effects can be modeled phenomenologically using multipliers to increase the plasma viscosity, heat conductivity, and electrical resistivity in the 1D MHD calculations. This procedure assumes that the implosion remains one dimensional on average even when the cause of the viscosity enhancements is an underlying fluid turbulence. These enhancements were found to soften z-pinch implosions (i.e., to lower the calculated plasma densities on axis) and to improve the agreement between z-pinch calculations and experiments [8]. A major effect of the implosion softening, also determined in Ref. [8], is to shift the breakpoint mass m_{BP} at which the transition from m^2 to m yield scaling occurs. We will reexamine the PI experiments from this new perspective. However, two new sets of experiments, similar to the PI experiments, were recently completed at the Saturn and Phoenix facilities of Sandia National Laboratories (SNL) and the Naval Surface Warfare Center (NSWC), respectively. These experiments will also be analyzed from the perspective of soft implosion z-pinch modeling. They have some of the features of the theoretically predicted yield behavior and some of the features of the PI experiments. However, they also have several points of disagreement both with theory and with each other that will be discussed in this paper.

In Sec. II, the K-shell yield scaling predictions of Ref. [1] are revised using information derived from Ref. [8]. The two velocity conditions that must be satisfied in order to efficiently convert plasma kinetic energy into K-shell x rays are conveniently displayed on a (m, v_f) plot, where v_f is the maximum array velocity achieved during implosion (theoretically, the final velocity achieved before the current is turned off). These conditions define regions in (m, v_f) space where efficient x-ray production can be achieved from different atomic number plasmas. The Saturn, Phoenix, and Double Eagle aluminum experiments are then described in Sec. III and analyzed in Sec. IV. These experiments probe through different portions of the efficient emission region, and a comparison of their yield data provides valuable interpretations of the different roles that the phase-1 and phase-4 pinch dynamics may be playing in each of the different sets of experiments. The locations of the maximum x-ray producing implosions in the Saturn and Phoenix experiments support the general validity of an x-ray scaling relation that was proposed in Ref. [1] for optimizing x-ray production from z-pinch plasmas. A somewhat modified version of this relation, which is supported by the data, is subsequently presented in Sec. IV. Finally, the significance of these experimental results is summarized in Sec. V and future problems discussed.

II. K-SHELL YIELD SCALING

While the dynamical characteristics of z-pinch implosions can be described in terms of the variables (m, v_f), their radiation capabilities are equivalently, but more conveniently, described in terms of two implosion ener-

gies, the kinetic energy per ion $K_i \equiv \frac{1}{2} m_i v_f^2$, where m_i is the mass of an ion, and the kinetic energy per centimeter $K_c \equiv \frac{1}{2} m v_f^2$. K_i determines the ability of the z-pinch load to radiate effectively from the K shell. We assume that K_i must be larger than the predetermined minimum energy $E_{\min}$, although kilovolt L-shell radiation losses may require K_i to be much larger than the $E_{\min}$ energy defined above. K_c, on the other hand, determines the quantity of radiation that can be produced. One can work interchangeably in terms of the variables $\{m, v_f\}$, $\{m, \eta\}$, or $\{K_c, K_i\}$.

Our present understanding of K-shell yield scaling has developed in a series of steps. Both hard and soft 1D implosion modeling have predicted approximately two K-shell scaling regimes, with a relatively sharp boundary between them. The scaling formulas that were developed from the hard implosion calculations are derived in Ref. [1]. We briefly summarize them here. For small masses, the K-shell x-ray yield y_K scales quadratically with mass,

$$y_K = a m^2 , \tag{1}$$

while for large masses, it scales approximately linearly,

$$y_K = b m . \tag{2}$$

The coefficients a and b are functions of Z and η, where Z is the atomic number of the wire array. The intersection of the two yield curves defines the breakpoint mass m_{BP} and the breakpoint yield y_{BP},

$$m_{\mathrm{BP}} = \frac{b}{a} , \quad y_{\mathrm{BP}} = \frac{b^2}{a} . \tag{3}$$

Approximate forms for the dependence of a and b on Z and η were worked out in Ref. [1]. They are based on $\eta \geq 3.9$ implosions and do not include the effects of soft implosion modeling to modify the inefficient region yield scaling as a function of η, or any dependence of the kinetic energy conversion efficiency in the efficient region on η. They also do not include kilovolt L-shell radiation losses, which become more and more important as Z increases. Only the effect of soft implosion modeling to shift the location of m_{BP} is included in this slightly revised summary of the dependence of a and b on Z and η [1]:

$$m_{\mathrm{BP}} \ (\mu\mathrm{g/cm}) = \frac{f_K b_0 Z^{5.96}}{a_0 E(Z)} , \tag{4}$$

$$y_{\mathrm{BP}} \ (\mathrm{kJ/cm}) = \frac{f_K^2 b_0^2 Z^{8.37}}{a_0 E(Z)} , \tag{5}$$

where f_K is the fractional conversion efficiency of kinetic energy to K-shell radiation in the efficient m scaling region. We will conservatively take f_K to be 0.3 when Eqs. (1) and (2) are used to plot theoretical yields on figures. The exponential factor E is defined by

$$E(Z) \equiv \exp(-20.6/Z^{0.9}) , \tag{6}$$

and the coefficients a, b, a_0, and b_0 by

$$a = a_0 E(Z) Z^{-3.55} , \quad b = f_K b_0 Z^{2.41} , \tag{7}$$

where

$$a_0 (\mathrm{kJ\,cm}/\mu\mathrm{g}^2) = \frac{1}{6} \left[33.7 + \frac{595}{\eta} - \frac{70.7}{\eta^2} \right] \tag{8}$$

and

$$b_0 \ (\mathrm{kJ}/\mu\mathrm{g}) = 9.1 \times 10^{-5} \eta . \tag{9}$$

Since the analysis in Ref. [8] showed that soft implosions shift the mass breakpoint (and broaden somewhat the transition between m^2 and m scaling), a correction factor of $\sim \frac{1}{6}$ is included in the a_0 equation to account for this effect. It increases m_{BP} by a factor of 6. The η dependence of a_0, shown in Eq. (8), was originally derived from a least squares fit of low mass yield, calculated behavior over the region $4 \leq \eta \leq 10$, and it should be extrapolated only with this limitation in mind outside of this range.

The above analysis provides two constraints on v_f that are necessary for efficient conversion of K_c to K-shell x rays in different elements. On the one hand, one must have $\eta > 1$ (possibly $\eta > 1.5$ or 2). On the other hand, one must have $m \geq m_{\mathrm{BP}}$. Hence the curves $\eta = \mathrm{const}$ and $m = m_{\mathrm{BP}}$ define the boundaries of a region in m-v_f space in which efficient x-ray emission can be achieved. Two of these regions, one for aluminum and one for krypton, are drawn in Fig. 1. The lower boundary curves are defined by $\eta = 1.5$. Figure 1 shows the different mass and implosion velocity requirements predicted by present theory that are needed in order to efficiently produce the 13–13.5 keV x rays that are emitted from the principal resonance lines in the K shell of krypton as opposed to the 1.6–1.7 keV lines that are emitted from the K shell of aluminum. Note again, however, that the present theory does not yet account for krypton's L-shell losses, which will strongly influence both the phase 2 and phase 3 pinch dynamics.

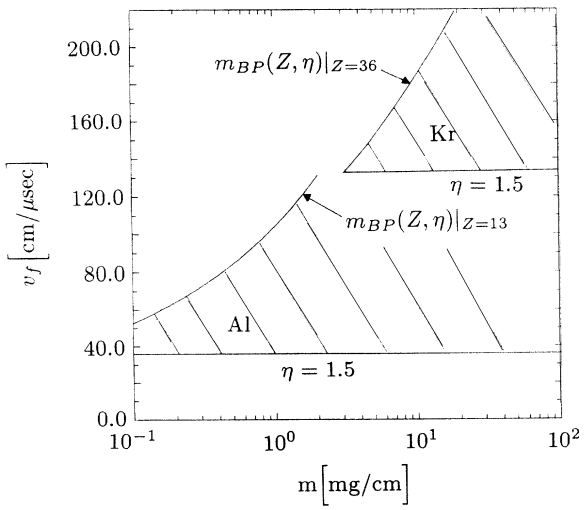

FIG. 1. Two shaded regions for aluminum and krypton defined by the boundary curves $\eta = 1.5$ and $m = m_{\mathrm{BP}}(\eta)$ are shown. In these regions, efficient conversion of z-pinch kinetic energy into K-shell emission is predicted to occur.

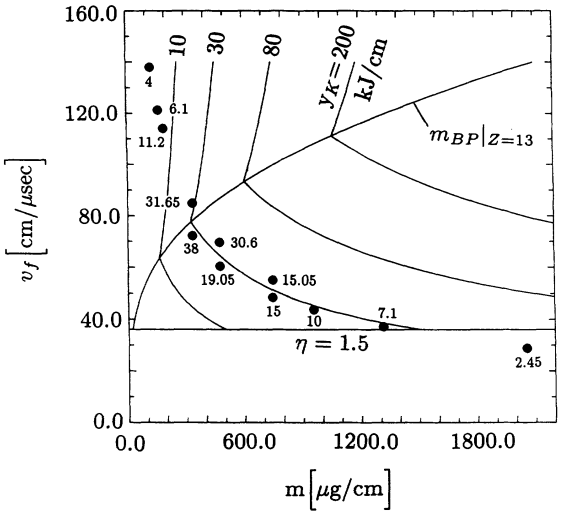

FIG. 2. The Saturn aluminum wire-array experiments listed in Table I are located relative to the efficient emission region for aluminum. Also displayed are the predicted yield contours for the generation of 10, 30, 80, and 200 kJ/cm of K-shell radiation through kinetic energy conversion as well as the measured yields/cm in each experiment.

The shaded regions in Fig. 1 indicate where efficient x-ray production is expected, but they do not show how the yield is predicted to increase as K_c (i.e., m or v_f) increases. This information is contained in Eqs. (1), (2), and (6)–(9) and can be displayed as contours on these figures. Predicted aluminum yield contours for 10, 30, 80, and 200 kJ/cm are shown in Figs. 2–4.

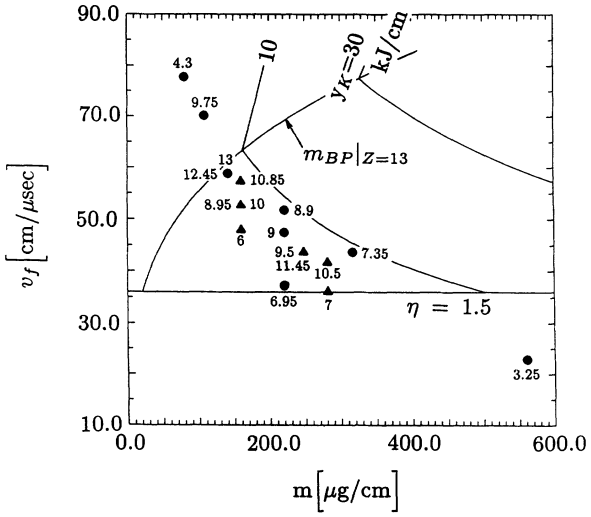

FIG. 3. The Phoenix aluminum wire-array experiments listed in Table II are located relative to the efficient emission region for aluminum. The circles are 16-wire-array shots and the triangles are 8-wire shots. Also displayed are the predicted yield contours for the generation of 10 and 30 kJ/cm of K-shell radiation through kinetic energy conversion as well as the measured yields/cm in each experiment.

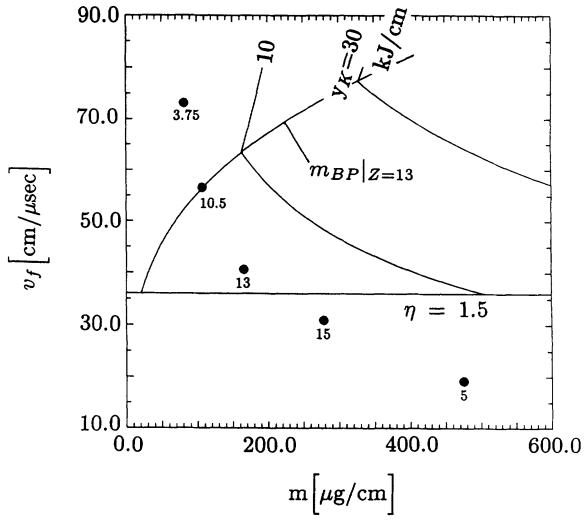

FIG. 4. The Double Eagle aluminum wire-array experiments listed in Table III are located relative to the efficient emission region for aluminum. Also displayed are the predicted yield contours for the generation of 10 and 30 kJ/cm of K-shell radiation through kinetic energy conversion as well as the measured yields/cm in each experiment.

III. SATURN, PHOENIX, AND DOUBLE EAGLE EXPERIMENTS

The experiments performed on the Saturn generator at SNL were originally designed to determine how the experimental results of the Double Eagle facility would scale to larger aluminum masses and implosion velocities. The experiments on the Phoenix facility at NSWC were designed to confirm whether or not the large x-ray conversion efficiencies that were seen on the Double Eagle facility could be duplicated with somewhat larger inputs of kinetic energy on a different, but similarly sized, pulse-power machine. Saturn is a much softer machine than the Double Eagle machine, i.e., the implosion induced by the current through the load reacts back on the current much more strongly in the Saturn than in the Double Eagle machine. Therefore, the Saturn experiments had to be designed using a lumped circuit model description of the electrical characteristics of the Saturn machine in order to drive the slug model calculations. The same procedure was used in designing the Phoenix experiments and for a reexamination of the Double Eagle experiments.

The circuit model we used is illustrated in Fig. 1 of Ref. [9]. The pulse-power generator is described by a time dependent voltage source $V(t)$ driving a line resistance Z_0, a line inductance L_p, and a dynamic z-pinch load with a time dependent inductance $L(r(t))$. A slug model of the dynamic load is used to determine $r(t)$, the location of the shell of imploding plasma. The load dynamics for the experiments were predicted, therefore, by solving the following two nonlinearly coupled equations [9]:

TABLE I. Saturn *z*-pinch experiments.

Wire diam (mil)	Array mass (μg/cm)	Array diam (cm)	η	Number of wires	KE (kJ)	Yield (kJ)	CE (%)
0.6	120	3.04	22	24	230	8.0	3.5
0.7	160	2.81	17	24	230	12.2	5.3
0.75	185	2.73	15	24	230	22.4	9.7
1.0	330	2.42	8.3	24	230	63.3	27.5
1.0	330	1.72	6.0	24	170	76.0	44.7
1.2	470	2.29	5.6	24	230	61.2	26.6
1.2	470	1.58	4.2	24	170	38.1	22.4
1.5	740	2.2	3.5	24	230	30.1	13.1
1.5	740	1.46	2.7	24	170	30.0	17.6
1.7	950	1.4	2.2	24	170	20.0	11.8
2.0	1310	1.34	1.6	24	170	14.2	8.4
2.5	2050	1.25	0.95	24	170	4.9	2.9

$$L_T\frac{dI}{dt}+\left[Z_0-L_0\frac{1}{r}\frac{dr}{dt}\right]I=V(t)\ , \tag{10}$$

$$m\frac{d^2r}{dt^2}=-\frac{L_0}{2l}I^2\frac{1}{r}\ . \tag{11}$$

In these equations, $I(t)$ is the current flowing through the circuit and the load, $L_T\equiv L_p-L_0\ln(r/r_0)$, $L_0\equiv(1-1/N)(\mu_0 l)/(2\pi)$, N is the number of wires in the array, l is the length of the array, and $\mu_0=4\pi\times10^{-7}$ H/m. The variable load inductance is given by $L=-L_0\ln(r/r_0)$. The implosion times predicted by this model are generally in accord with experiment. In this circumstance, one can assume that the calculated total kinetic energies and kinetic energies per ion will also be in close accord with the respective experimental energies.

A detailed listing of the experimental parameters used in the Saturn and Phoenix experiments is given in Tables I and II. Commercial aluminum wires were used in these experiments. On the Saturn machine, the arrays contained 24 wires, while on the Phoenix machine, a mix of 8- and 16-wire arrays was used. In both sets of experiments, the arrays were 2 cm in length. The two theoretical parameters in the tables, η and KE, which represents $K_T\equiv K_c l$, were calculated by terminating the solutions to Eqs. (1) and (2) in each case at $r(t_{\rm imp})=1.5$ mm, where $t_{\rm imp}$ is by definition the implosion time. The (K-shell) total yields in these tables, on the other hand, were measured, and each percent conversion efficiency (CE) that is listed is the ratio of measured yield to computed kinetic energy.

The yields in Table II were obtained by averaging yield measurements from several data channels. In this way, if one channel failed to function properly, it could be eliminated from the average. However, in one case, that of the 12 kJ yield listed for the 158 μg/cm shot at an initial array diameter of 1.7 cm, an entire type of yield diagnostic was missing. The listed yield was, therefore, corrected for the estimated effect of the missing diagnostic channels relative to the other shots.

TABLE II. Phoenix *z*-pinch experiments.

Wire diam (mil)	Array mass (μg/cm)	Array diam (cm)	η	Number of wires	KE (kJ)	Yield (kJ)	CE (%)
0.6	79	2.62	7.0	16	46	8.6	18.7
0.7	107	2.58	5.7	16	52	19.5	37.5
0.8	140	2.25	4.0	16	48.5	26	54
0.8	140	2.25	4.0	16	48.5	24.9	51.3
1.2	158	2.35	3.8	8	52	21.7	41.7
1.2	158	2.0	3.2	8	43.5	20	46
1.2	158	2.0	3.2	8	43.5	17.9	41.1
1.2	158	1.7	2.65	8	36	12	33
1.0	219	2.4	3.1	16	59	17.8	30.2
1.0	219	2.1	2.6	16	55	18	33
1.0	219	1.44	1.6	16	31	13.9	44.8
1.5	246	1.9	2.2	8	46	22.9	49.8
1.5	246	1.9	2.2	8	46	19	41
1.6	280	2.0	2.0	8	49	21	43
1.6	280	1.5	1.5	8	37	14	38
1.2	315	2.26	2.2	16	60	14.7	24.5
1.6	560	1.15	0.6	16	31	6.5	21

A similar table is constructed for five of the Double Eagle experiments of Ref. [3] in Table III. In these experiments, the arrays were also 2 cm in length, and they consisted of 12 wires. The array and wire diameters and the array masses are taken from Ref. [3], but η and the total kinetic energies, which, in Ref. [3], were inferred from the experiments, were calculated from Eqs. (1) and (2) using a lumped electrical circuit model for the Double Eagle machine. The (K-shell) yields were measured, and the conversion efficiencies are computed as stated above.

In three Saturn cases, the same mass was imploded in two different experimental shots to different final velocities. In one case, (the 330 μg/cm load) the yield went down when η increased; in the other two cases involving 470 and 740 μg/cm loads, the yield increased with η, although this is a marginal claim for the 740 μg/cm experiments. On the Phoenix machine, five cases were investigated in which m was held constant and η was varied. In three of these cases involving 140, 158, and 246 μg/cm loads, identical experiments were performed, and the reproducibility of the 8- and 16-wire-array implosions was tested. The measured yields differed roughly by 10%, 5%, and 20%, respectively, in these cases. In the other Phoenix experiments where the same mass was accelerated to higher velocities, the yield increased as v_f increased in all cases within the reproducibility of the experiments, i.e., the $\eta=3.1$ and $\eta=2.6$ shots involving the 219 μg/cm load were the exception, but the measured yields were essentially indistinguishable to within experimental error.

In Tables I–III, the experiments are listed in order of increasing load mass and decreasing η. The computed x-ray conversion efficiencies are highest for the Double Eagle experiments and roughly a factor of 2 less for the Phoenix than for the Double Eagle machine, and they were lowest for the Saturn machine. This ordering is the same as the ordering of the current rise times of the generators; namely, the current reaches its peak value into a short circuit load in 50 nsec on Saturn, in 100 ns on Phoenix, and in 125 ns on Double Eagle. This relationship suggests that there is more of an overlap between the phase-1 and phase-2 dynamics of array implosions on Saturn than on Double Eagle. A stronger case for this interaction can be made by comparing the wire explosion behavior predicted by a self-similar hydrodynamics model [10] to the observed yield behavior on Saturn and Double Eagle [11]. When the Saturn yield data in Table I are plotted as a function of array diameter as in Ref. [11], a dip in the yield is seen at an array diameter of 2.2 cm. This dip is correlated with a similar rise in the wire ion density that is generated halfway into the current rise by the wire explosion. The self-similar model used in the calculation of these ion densities assumes that the wire expansion is uniform and that it is driven by a time-evolving isothermal plasma. It predicts a significant correlation between the ion densities that are generated during wire explosion and the yields that are generated on axis. This work is published in Ref. [11] and will not be reported on here.

IV. DISCUSSION

The Saturn, Phoenix, and Double Eagle experiments were designed to probe through the efficient K-shell emission region of aluminum, which is shown in Fig. 1. Each experiment can be plotted as a point in m-v_f space using the relationship

$$v_f=\sqrt{3.242\eta/(10^{24}m_i)}Z^{1.831}\text{cm}/\mu\text{sec}\ ,$$

and the η values listed in Tables I–III. These experimental points are shown in Figs. 2–4 for Tables I–III, respectively, along with contours for the K-shell yields that are predicted by Eqs. (1), (2), and (6)–(9). The contours were drawn assuming a constant, conservative conversion efficiency f_K of 0.3 These predictions are considered conservative since they do not as yet include energy delivery to the load that might occur after stagnation or increases in f_K that occur as a function of m [1]. Note that each generator is capable of probing through the efficient emission region of aluminum over a wide range of (m,v_f) values, but that each machine can probe only over more limited ranges of variable m and constant v_f or variable v_f and constant m.

As noted in Sec. II, several cases in which the same mass was accelerated to a variety of final velocities are represented in the Saturn and Phoenix data. In the Phoenix experiments, all of these cases lay within the efficient region, and, in all of these experiments, the observed yield increased (or did not decrease) as v_f increased in conformity with theoretical predictions. The same behavior was seen in the 470 and 740 μg/cm shots on the Saturn machine. However, for the 330-μg/cm shots, which lay near the $m=m_{\text{BP}}$ boundary with one experiment lying above and one below the boundary, the reverse was true; namely, the yield went down as the implosion velocity increased (again in conformity with theory). As the yield contours in Figs. 2–4 show, this behavior is

TABLE III. Double Eagle z-pinch experiments.

Wire diam (mil)	Array mass (μg/cm)	Array diam (cm)	η	Number of wires	KE (kJ)	Yield (kJ)	CE (%)
0.7	80	2.5	6.2	12	43	7.5	17
0.8	105	2.0	3.7	12	33.5	21	63
1.0	164	1.5	1.9	12	27	26	96
1.3	277	1.25	1.1	12	26	30	115
1.7	474	0.9	0.42	12	17	10	59

indicative of yield behavior in the inefficient region where $\eta > 1$. These observations must be made with a note of caution since there is experimental uncertainty in the data and more experimental shots are needed to reduce this uncertainty. However, this yield behavior as a function of η must be utilized in order to experimentally map out the boundaries of the efficient emission region.

The *K*-shell yields corresponding to each of the Figs. 2–4 experiments are plotted in Figs. 5–7, respectively, and they demonstrate a major point of difference between the Double Eagle and the Saturn and Phoenix experiments. In sharp contrast to the Double Eagle experiment, maximum yields in both the Saturn and Phoenix experiments were attained when the experiments lay within the efficient region, but were adjacent to the $m = m_{BP}$ boundary curve as predicted by theory (see Ref. [1]). Moreover, as also predicted, yields fell as the implosion velocity was increased and the experiments were moved further from the efficient region. Similarly, as the implosion velocity was decreased, moving the experiments towards and ultimately below the $\eta = 1.5$ boundary line, the yields fell. Since the yield contours that are drawn in Figs. 2–4 were derived from hard implosion calculations (corrected only for the mass breakpoint shift), they do not show the same drop in yield with η for constant $m\eta$ that is seen in the Saturn and Phoenix data. However, soft implosion calculations [8] do show this trend.

The Phoenix data also suggests that the number of wires used in the experiments may be a potentially important influence on the x-ray yield depending on the location of the wires relative to the return current posts. The yields from the eight-wire Phoenix shots are plotted as triangles in Fig. 6, while the 16-wire shots are plotted as circles. The behavior of the 16-wire yields on the Phoenix machine closely corresponds to the behavior of the 24-wire shots on the Saturn machine. The eight-wire shots, on the other hand, appear to have a trend line that more closely resembles the Double Eagle data. These trends may indicate the influence of different $\mathbf{J} \times \mathbf{B}$ forces acting on the wires depending on the number of return current posts and on the location of the wires relative to the posts. The Saturn machine has eight posts, Phoenix eight, and Double Eagle six. In the Saturn and Double Eagle experiments, the position of the wires relative to the current returns was not held constant, but they were randomly placed. By contrast, in the eight-wire Phoenix experiments, the wires were positioned along the same radii as the posts, while in the 16-wire shots, they were rotated to lie symmetrically opposed to the posts.

In spite of their qualitatively similar behavior, Saturn and Phoenix *K*-shell yield data have an important quanti-

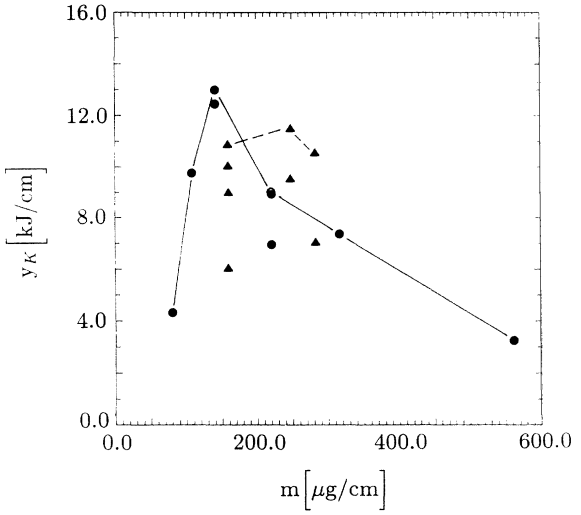

FIG. 6. The measured *K*-shell yields in the Phoenix experiments, which are listed in Table II, are plotted as a function of the aluminum array mass per cm. The circles are 16-wire-array shots, and the triangles are 8-wire shots.

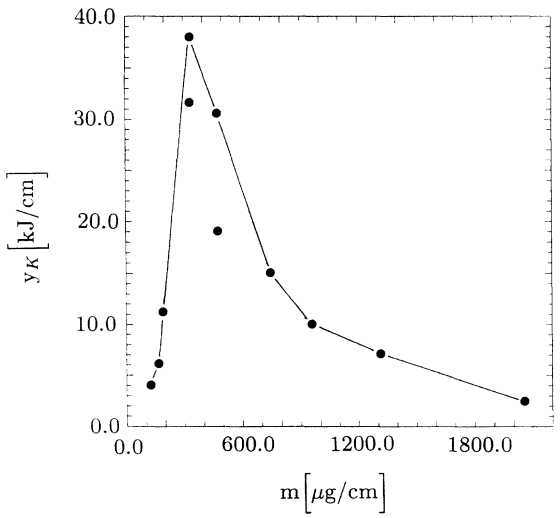

FIG. 5. The measured *K*-shell yields in the Saturn experiments, which are listed in Table I, are plotted as a function of the aluminum array mass per cm.

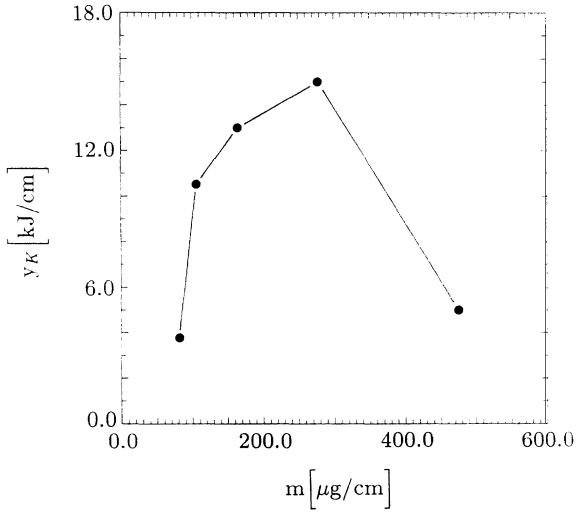

FIG. 7. The measured *K*-shell yields in the Double Eagle experiments, which are listed in Table III, are plotted as a function of the aluminum array mass per cm.

tative difference. All of the Phoenix shots within the efficient region had conversion efficiencies greater than the theoretically predicted, conservative, 30% value. For the Saturn machine, however, only the maximum yielding of the experiments within this region exceeded 30%. Nevertheless, in this one case, the 45% conversion efficiency observed on the Saturn machine equaled the Phoenix maximum efficiency of 54% to within the range of the experimental variability of the two machines.

The Saturn and Phoenix data provide support, albeit somewhat preliminary, for one of the important predictions in Ref. [1] dealing with the dependence of the maximum yield on load mass. In both sets of experiments, the shots with maximum yield were located near the $m=m_{\mathrm{BP}}$ boundary. In this case, the predicted dependence of K-shell yield on load mass is

$$y_K=y_{\mathrm{BP}}\equiv y_K(m)|_{m=m_{\mathrm{BP}}}\equiv y_{\mathrm{BP}}(m_{\mathrm{BP}}) .$$

In Ref. [1], a least squares fit to three theoretical data points, covering the span $2.5\leq\eta\leq 28$, produced the result $y_K\propto m^{1.7}$. This result was derived from three sets of calculations in which m was held constant and η was varied. In each case, an η value was found at which the K-shell yield attained a maximum value. Clearly, if viewed on an m-v_f plot, this maximum occurs at $m=m_{\mathrm{BP}}$. Thus one can use the mass breakpoint curve to predict the maximum K-shell yields $y_K^{\max}$ from aluminum that are based on kinetic energy conversion alone. From Eqs. (4)–(9) (and as a check on their accuracy), one can find the following least squares fit to the $y_K^{\max}=y_{\mathrm{BP}}(m_{\mathrm{BP}})$ curve over the range $1.5\leq\eta\leq 10$:

$$y_K^{\max}\ (\mathrm{kJ/cm})=4.36\times 10^{-3}m^{1.565} \tag{12}$$

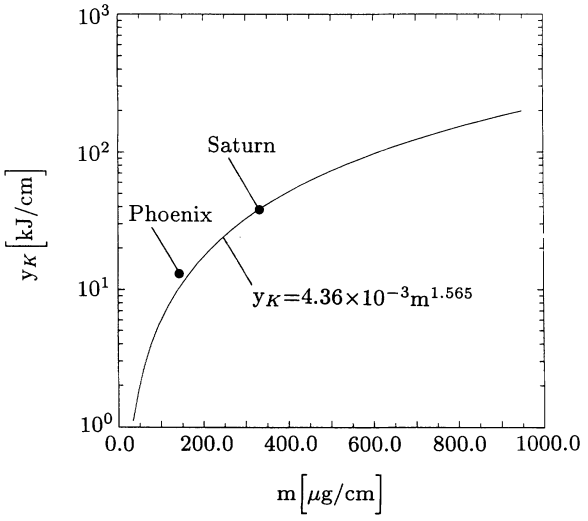

FIG. 8. A least squares fit to the theoretical curve $y_K=y_{\mathrm{BP}}(\eta(m_{\mathrm{BP}}))$, is plotted as a function of m_{BP}. Also shown are the maximum yielding of the Phoenix and Saturn shots, which were located adjacent to the $m=m_{\mathrm{BP}}$ curve, as predicted. The least squares fit is obtained for and plotted over the range $1.5\leq\eta\leq 10$.

for $f_K=0.5$ and m in units of μg/cm. It is drawn in Fig. 8, and the Phoenix and Saturn data points for the maximum yields are included on the figure for comparison. As an aside, Fig. 1 shows that the $m=m_{\mathrm{BP}}$ curves do not depend strongly on Z. A least squares fit covering the ranges $10\leq Z\leq 36$ and $1.5\leq\eta\leq 10$ produces the formula

$$y_{\mathrm{BP}}=0.004\,84m_{\mathrm{BP}}^{1.534} , \tag{13}$$

when $f_K=0.5$.

V. SUMMARY AND CONCLUSIONS

When slug models of the load dynamics of z-pinch plasmas are used to design and interpret z-pinch experiments, useful classifications can be made of the role of kinetic energy on the overall K-shell emission characteristics of the pinch. However, the slug model is an idealized description of the implosion, and it must be applied with caution. Moreover, it provides no direct information about the emission characteristics of the pinch. For this information, one must employ radiative hydrodynamics calculations that, at minimum, take into account the opacity and the photoexcitation dynamics of the plasma. As discussed in this paper, 1D radiative hydrodynamic calculations provide the basis for the yield scaling predictions. These calculations begin with a given mass of preionized cylindrically symmetric plasma tightly located, on average, at the initial position of a wire array. Thus two basic assumptions underlie the application of these calculations to the analysis and interpretation of z-pinch experimental data; namely, (1) that the power flow from the pulsed-power machine couples effectively to the wire load to ionize it quickly and uniformly and (2) that the wire-array implosion then takes place with all of the wire mass, which one distributes symmetrically within the cylinder of the calculation, imploding inwards driven by the $\mathbf{J}\times\mathbf{B}$ forces of the discharge. These assumptions essentially validate the slug model description of the implosion; however, they are not always justified. There are strong indications that large diameter wires do not ionize uniformly, that some of the wire mass is left behind in the implosion, and that the mass is driven in under a combination of slug and snowplow dynamics. (In a slug model implosion, all of the load mass is assumed to have the same acceleration, while in a snowplow implosion, mass is swept up and accelerated continuously as the implosion proceeds.) The first two of these phenomena are suggested by experiments [12], and the third by a recent analysis of PI data [8,13]. Moreover, at higher input power levels, L- and M-shell radiation losses during implosion may further invalidate a slug model description of the dynamics even when all of the load mass implodes.

Some or all of these considerations may explain the mutual discrepancies, among Saturn, Phoenix, and Double Eagle yield data and the yield predictions. For example, Double Eagle data show evidence of anomalous heating taking place on axis that neither the Saturn nor Phoenix data exhibit. Phoenix yield conversion efficiencies agree reasonably well with predictions in the efficient region, while Saturn and Double Eagle data do not—especially for low η values. Saturn and Phoenix

yield data have peaks near the mass breakpoint boundary, a peak that Double Eagle data do not have. Finally, Saturn conversion efficiencies do not measure up to theoretical expectations in all but one shot, while the Phoenix and Double Eagle data equal or exceed these expectations.

The kinetic energy conversion efficiencies in the three sets of experiments are correlated with the times to peak current into a short-circuit load of the three machines (ignoring prepulses); Double Eagle has the longest short-circuit current rise time and the largest conversion efficiencies while Saturn has the shortest rise time and the smallest conversion efficiencies. In the Saturn experiments, implosion times between 64 and 99 nsec were measured. These implosions occur around the peak in the short-circuit current at 70 nsec. In the Phoenix experiments, the loads reached the axis in 75–95 nsec, either before or at the time of peak short-circuit current. However, in the Double Eagle experiments, the loads imploded in 85–95 nsec, well before the short-circuit current peak. This may explain the Double Eagle machine's apparent ability to deliver a significant amount of energy to the load during the phase-4 dynamics, which, evidently, neither Saturn nor Phoenix was able to do.

There were four ways, however, in which the above experiments confirmed theoretical expectations. On each machine, for example, the theoretically predicted minimum conversion efficiency was exceeded in at least one case. It happened only once on the Saturn machine, but in several other cases the conversion was near 30%. Second, in both Saturn and Phoenix experiments, the yield increased as a function of η for fixed m in the efficient region. Third, in all experiments to varying degrees, the location of the mass breakpoint boundary was determined in agreement with soft implosion hydrodynamics modeling. The Phoenix and Double Eagle experiments also demarked the lower ($\eta > 1$) boundary of the efficient emission region fairly well. Finally, both Saturn and Phoenix yields peaked at the mass breakpoint boundary. Because of this behavior, the approximate scaling law for maximum K-shell emission as a function of load mass, derived in Ref. [1], was approximately validated. This scaling assumes that the pinch does not receive any additional energy input of significance while on axis.

The theoretical K-shell yield scaling developed to date is based on calculations in which the current is terminated prior to load assembly on axis. These calculations have a number of defects or limitations, some of which have been mentioned above. Since the load current does not shut off in most experiments, it is necessary, for example, to extend the scaling laws utilizing current-on calculations. Maintaining the current not only increases the confinement of the pinch, but it can also promote the pinch's radiative collapse. Both of these phenomena may lead to increases in radiative output. The experiments described in this paper have helped to confirm that the m_{BP} boundary, recently redefined by soft implosion modeling, is reasonably well placed. Additional experiments are needed to determine this boundary more accurately for aluminum (and other higher-Z elements) as well as to determine aluminum's yield contours within the efficient and inefficient emissions regions. The main defining characteristic of the efficient region is that x-ray yields will increase with v_f for a fixed m. Outside of this region when $\eta > 1$, yields and conversion efficiencies fall as v_f increases for fixed m because the plasma ionizes progressively more rapidly through the K shell. Finally, the $\eta = 1$ boundary was best defined in the Double Eagle and Phoenix experiments and less well defined in the Saturn experiments. More experiments are needed in order to determine whether this latter effect is related to the overlap of the wire explosion and implosion dynamics on the Saturn machine.

ACKNOWLEDGMENTS

The authors would like to thank J. P. Apruzese for several discussions and useful comments on this paper.

[1] K. G. Whitney, J. W. Thornhill, J. P. Apruzese, and J. Davis, J. Appl. Phys. **67**, 1725 (1990).

[2] J. W. Thornhill, K. G. Whitney, and J. Davis, J. Quant. Spectrosc. Radiat. Transfer **44**, 251 (1990).

[3] C. Deeney, T. Nash, R. R. Prasad, L. Warren, K. G. Whitney, J. W. Thornhill, and M. C. Coulter, Phys. Rev. A **44**, 6762 (1991).

[4] P. M. Bellan, Phys. Rev. Lett. **69**, 3515 (1992).

[5] N. B. Volkov, T. A. Golub, N. A. Gondarenko, and A. M. Iskoldsky, in *Proceedings of the 9th International Conference on High-Powered Particle Beams, Washington, DC,* edited by D. Mosher and G. Cooperstein (NTIS, Springerfield, VA, 1992), p. 575.

[6] T. W. Hussey, N. F. Roderick, and D. A. Kloc, J. Appl. Phys. **51**, 1452 (1980).

[7] T. A. Zang, R. B. Dahlburg, and J. P. Dahlburg, Phys. Fluids A **4**, 127 (1992).

[8] J. W. Thornhill, K. G. Whitney, C. Deeney, and P. D. LePell, Phys. Plasmas **1**, 321 (1994).

[9] J. Katzenstein, J. Appl. Phys. **52**, 676 (1981).

[10] H. W. Bloomberg, M. Lampe, and D. G. Colombant, J. Appl. Phys. **51**, 5277 (1980).

[11] K. G. Whitney, J. W. Thornhill, R. B. Spielman, T. J. Nash, J. S. McGurn, L. E. Ruggles, and M. C. Coulter, in *Dense Z-pinches,* Third International Conference, London, 1993, edited by M. Haines and A. Knight, AIP Conf. Proc. No. 299 (AIP, New York, 1994), p. 429.

[12] I. K. Aivazov, V. D. Vikharev, G. S. Volkov, L. B. Nikandrov, V. P. Smirnov, and V. Ya. Tsarfin, Fiz. Plazmy **14**, 197 (1988) [Sov. J. Plasma Phys. **14**, 110 (1988)].

[13] C. Deeney, P. D. LePell, B. H. Failor, J. S. Meachum, S. Wong, J. W. Thornhill, K. G. Whitney, and M. C. Coulter, J. Appl. Phys. **75**, 2781 (1994).